Hierarchical Design of Connected Cruise Control in the Presence of Information Delays and Uncertain Vehicle Dynamics

Linjun Zhang, Jing Sun, *Fellow, IEEE*, and Gábor Orosz

***Abstract*— In this paper, we investigate the design of connected cruise control that exploits wireless vehicle-to-vehicle communication to enhance vehicle mobility and safety. A hierarchical framework is used to reduce the complexity for design and analysis. A high-level controller incorporates the motion data received from multiple vehicles ahead and also considers information delays, in order to generate the desired longitudinal dynamics. At the lower level, we consider a physics-based vehicle model and design an adaptive sliding-mode controller that regulates the engine torque, so that the vehicle can track the desired dynamics in the presence of uncertainties and external perturbations. Numerical simulations are used to validate the analytical results and demonstrate the robustness of the controller.**

***Index Terms*— Adaptive sliding-mode control, connected cruise control (CCC), time delay, vehicle-to-vehicle (V2V) communication.**

I. Introduction

IN RECENT years, increasing attention has been paid to advanced driver assistance systems (ADASs) and autonomous driving [1], [2], in order to enhance vehicle safety and improve the comfort of passengers. Most of the existing ADAS applications rely on camera and range sensors (e.g., radar and LIDAR) that can only detect the objects within the line of sight. However, emerging wireless vehicle-to-vehicle (V2V) communication can be used to monitor the vehicles beyond the line of sight, and, thus, has potentials for improving vehicle safety and mobility.

One way to implement V2V communication in vehicle control systems is to construct cooperative adaptive cruise control (CACC) [3], which forms a vehicle platoon where each vehicle automatically follows the vehicle immediately ahead relying on range sensors and also responds to the motion of the designated platoon leader using V2V communication. A large number of theoretical studies have been conducted to investigate the impacts of CACC on traffic flow dynamics. Results in [4] and [5] showed that CACC could increase the traffic capacity by allowing smaller intervehicle distances. In [6] and [7], CACC was designed by considering the information delays caused by intermittency and packet drops in V2V communication. Experiments were also carried out to evaluate the performance of CACC in practice [8]–[11]. Although CACC has potentials for increasing traffic capacity and enhancing vehicle safety, its implementation in real traffic may be difficult. First, CACC is designed for vehicle platoons rather than individual vehicles. Thus, to achieve the desired performance, the realization of CACC requires that multiple vehicles equipped with autonomous driving systems travel next to each other, which rarely occurs, in practice, due to the low penetration of such vehicles. Moreover, CACC requires all vehicles to communicate with the designated platoon leader, which restricts the connectivity topology and also restricts the platoon length by the communication range.

Relaxing the aforementioned restrictions of CACC, we proposed the concept of connected cruise control (CCC) [12]–[14], which allows the incorporation of human-driven vehicles that may not broadcast information. Moreover, CCC requires neither a designated leader nor a prescribed connectivity topology. Indeed, camera and range sensors are not required for implementing CCC, although integrating these sensors with V2V communication can enhance reliability and safety. These relaxations make CCC more flexible and scalable for implementation in real traffic. Mixing CCC vehicles into traffic flow of human-driven vehicles leads to vehicle networks that may have complex connectivity topologies. In [15], the impact of connectivity topologies on the stability of vehicle networks was investigated while the dynamics of all vehicles were assumed to be identical and the information delays were neglected. However, information delays arising from intermittency and packet drops in wireless communication have significant influence on the dynamics of vehicle networks. In [12] and [16], the influences of connectivity topologies, information delays, and nonlinear dynamics on the stability of vehicle networks were studied based on a simplified vehicle model. In these works, physical effects, such as rolling resistance and aerodynamic drag, were neglected for simplicity, but such disturbances may significantly affect the vehicle dynamics and the subsequent CCC design [14]. Moreover, the vehicle parameters (e.g., mass, aerodynamic drag coefficient, and rolling resistance coefficient) are uncertain in practice and they may vary under different conditions.

Manuscript received March 28, 2016; revised October 3, 2016; accepted January 7, 2017. Date of publication February 21, 2017; date of current version December 14, 2017. Manuscript received in final form January 31, 2017. This work was supported by the National Science Foundation under Award 1351456. Recommended by Associate Editor C. Canudas-de-wit.

L. Zhang and G. Orosz are with the Department of Mechanical Engineering, University of Michigan, Ann Arbor, MI 48109 USA (e-mail: linjunzh@umich.edu; orosz@umich.edu).

J. Sun is with the Department of Naval Architecture and Marine Engineering, University of Michigan, Ann Arbor, MI 48109 USA (e-mail: jingsun@umich.edu).

Color versions of one or more of the figures in this paper are available online at http://ieeexplore.ieee.org.

Digital Object Identifier 10.1109/TCST.2017.2664721

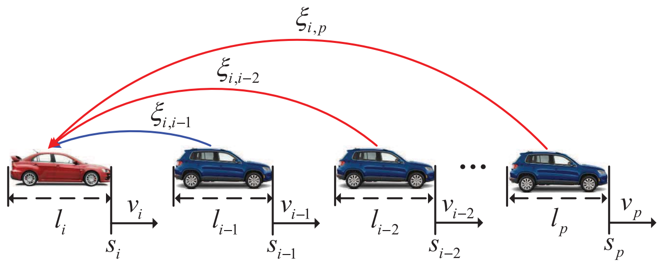

Fig. 1. Vehicle network where a CCC vehicle (red) at the tail receives information broadcasted by multiple vehicles ahead. The symbols s_j, l_j, and v_j denote the position, length, and velocity of vehicle j, respectively, while $\xi_{i,j}$ denotes the information delay between vehicles i and j.

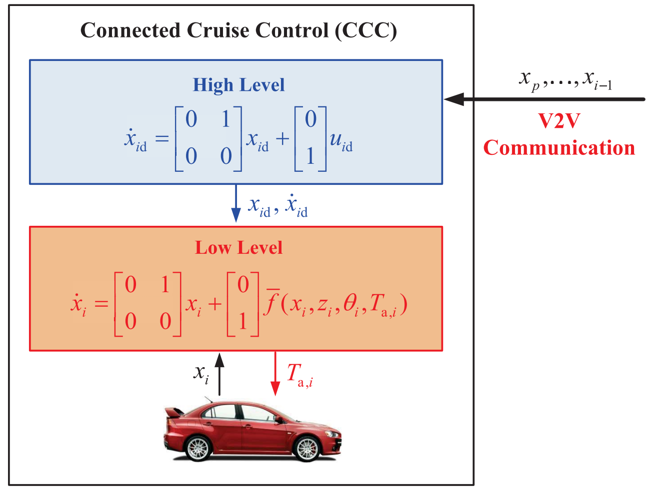

Fig. 2. Hierarchical framework for CCC design. The high-level controller u_{id} is designed to generate the desired state x_{id} for the CCC vehicle i by incorporating the motion data x_j received from vehicles $j = p, \ldots, i-1$. At the low level, a physics-based vehicle model is used to design a control strategy for the axle torque $T_{a,i}$, such that the CCC vehicle can track the desired state x_{id}. Here, z_i is a vector consisting of external disturbances, such as road angle and headwind speed, while the vector θ_i contains all vehicle parameters (e.g., vehicle mass, rolling resistance coefficient, aerodynamic drag coefficient, and so on).

CCC design in the presence of information delays and uncertain vehicle dynamics is a challenging problem. To address this problem, in this paper, we present a hierarchical framework that reduces the complexity of CCC design and analysis. The high-level controller exploits the time-delayed data received from vehicles ahead and generates the desired longitudinal dynamics, while the low-level controller regulates the engine torque, such that the vehicle can track the desired motion in the presence of uncertainties. In particular, at the high level, we present a general framework that provides guidelines for designing a large variety of either linear or nonlinear controllers. This differs from the existing works [6], [7], [12], [16] that investigated specific controllers. At the low level, we design an adaptive sliding-mode controller that guarantees tracking performance in the presence of uncertain external disturbances, which were not considered in previous works [17]–[19]. Numerical simulations are conducted to validate the analytical results and evaluate the system performance.

The rest of this paper is organized as follows. In Section II, a hierarchical framework is presented for CCC design and corresponding stability conditions are derived. We conduct a case study in Section III where a CCC vehicle whose controller is designed by using the proposed framework is embedded in a vehicle network, and numerical simulations are used to evaluate the system performance. In Section IV, we summarize our results and discuss future work.

II. Hierarchical Framework for Connected Cruise Control

CCC algorithms are designed by incorporating the motion data received from multiple vehicles ahead, in order to achieve system-level properties, such as string stability [20], optimal fuel efficiency [11], and collision avoidance [21]. For reliable implementation in practice, CCC must be designed by considering information delays, connectivity topologies, nonlinear vehicle dynamics, and uncertainties. In this section, we present a hierarchical CCC framework, in order to simplify the design and analysis.

Fig. 1 shows a vehicle network where the CCC vehicle i (red) monitors the positions s_j and the velocities v_j of vehicles $j = p, \ldots, i-1$, where p denotes the furthest vehicle within the communication range of vehicle i. In particular, we assume that the position s_j is measured at the front bumper of vehicle j. The length of vehicle j is denoted by l_j. The symbol $\xi_{i,j}$ denotes the information delay between vehicle i and vehicle j, which may be caused by human reaction time, delay in range sensors, or intermittency and packet drops in V2V communication. Note that vehicle $i-1$ may be monitored by human perception, range sensors, or V2V communication, while the distant vehicles $j = p, \ldots, i-2$ can only be monitored by using V2V communication, since they are beyond the line of sight.

We emphasize that CCC allows the incorporation of vehicles that do not broadcast information, which leads to a large variety of connectivity topologies. Also, information delays between different pairs of vehicles may have different values. Moreover, there exist uncertain parameters and disturbances in vehicle dynamics. It is a challenging problem to design CCC that is robust against connectivity topologies, information delays, and uncertain vehicle dynamics. To reduce the complexity of CCC design, we exploit a hierarchical framework, as shown in Fig. 2, where the desired state of vehicle i and the actual state of vehicle j are defined by

$$x_{id} = \begin{bmatrix} s_{id} \\ v_{id} \end{bmatrix}, \quad x_j = \begin{bmatrix} s_j \\ v_j \end{bmatrix} \tag{1}$$

respectively, for $j = p, \ldots, i$. At the high level, we consider a simplified vehicle model

$$\dot{x}_{id} = \begin{bmatrix} 0 & 1 \\ 0 & 0 \end{bmatrix} x_{id} + \begin{bmatrix} 0 \\ 1 \end{bmatrix} u_{id} \tag{2}$$

and design the desired acceleration u_{id} to determine the desired state x_{id} by incorporating the motion data $x_p, \ldots, x_{i-1}$. At the low level, a physics-based vehicle model

$$\dot{x}_i = \begin{bmatrix} 0 & 1 \\ 0 & 0 \end{bmatrix} x_i + \begin{bmatrix} 0 \\ 1 \end{bmatrix} \overline{f}(x_i, z_i, \theta_i, T_{a,i}) \tag{3}$$

is used to design the axle torque $T_{a,i}$, such that the vehicle state x_i can track its desired state x_{id}. Here, the vector z_i contains external disturbances, such as road inclination angle and headwind speed while the vector θ_i consists of all vehicle parameters, such as vehicle mass, aerodynamic drag coefficient, and rolling resistance coefficient. In practice, there exist uncertainties in parameters and disturbances. Hence, the low-level controller must guarantee the tracking performance while counteracting the uncertainties arising from vehicle dynamics.

A. High Level: Connected Car-Following Dynamics

At the high level, we use the model (2) to design the connected car-following dynamics by incorporating the motion data received from multiple vehicles ahead, in order to achieve system-level properties, such as collision avoidance and minimal fuel consumption. These properties require the asymptotic stability of the uniform flow equilibrium. That is, if vehicles $j = p, \ldots, i-1$ move at the same constant speed v^* while keeping the same constant distances h^* from the vehicle immediately ahead, that is

$$x_j^*(t) = \begin{bmatrix} s_j^*(t) \\ v_j^*(t) \end{bmatrix} = \begin{bmatrix} v^* t + \bar{s}_j \\ v^* \end{bmatrix} \tag{4}$$

for $j = p, \ldots, i-1$ with $\bar{s}_{j-1} - l_{j-1} - \bar{s}_j = h^*$, then the state of the CCC vehicle i shall approach the equilibrium

$$x_{id}^*(t) = \begin{bmatrix} s_{id}^*(t) \\ v_{id}^*(t) \end{bmatrix} = \begin{bmatrix} v^* t + \bar{s}_{id} \\ v^* \end{bmatrix} \tag{5}$$

where $\bar{s}_{i-1} - l_{i-1} - \bar{s}_{id} = h^*$.

Incorporating the time-delayed information received from multiple vehicles ahead, we propose a high-level controller for the CCC vehicle i in the form

$$u_{id}(t) = \sum_{j=p}^{i-1} \gamma_{i,j}\big(f_{i,j}(h_{id,j}(t-\xi_{i,j})) + g_{i,j}(v_{id}(t-\xi_{i,j})) + d_{i,j}(v_j(t-\xi_{i,j}))\big) \tag{6}$$

see Fig. 1, where the constants $\gamma_{i,j}$ determine the connectivity topology of information flow, such that

$$\gamma_{i,j} = \begin{cases} 1, & \text{if vehicle } i \text{ uses data of vehicle } j \\ 0, & \text{otherwise.} \end{cases} \tag{7}$$

The quantity

$$h_{id,j}(t) = \frac{s_j(t) - s_{id}(t) - \sum_{k=j}^{i-1} l_k}{i-j} \tag{8}$$

represents the average bumper-to-bumper distance between vehicles i and j. At the uniform flow equilibrium, we have

$$h_{id,j}^* = \frac{s_j^*(t) - s_{id}^*(t) - \sum_{k=j}^{i-1} l_k}{i-j} = h^* \tag{9}$$

for $j = p, \ldots, i-1$; see (4) and (5).

In (6), the term $f_{i,j}(h_{id,j})$ denotes the response to the average distance while the terms $g_{i,j}(v_{id})$ and $d_{i,j}(v_j)$ represent the responses to the velocity of vehicle i and that of vehicle j, respectively. We remark that these functions must satisfy the following properties.

P1 Functions $f_{i,j}(h)$, $g_{i,j}(v)$, and $d_{i,j}(v)$ are continuously differentiable with respect to their arguments.

P2 The function $f_{i,j}(h)$ is a monotonically increasing function of h.

P3 The relation

$$f_{i,j}(h^*) + g_{i,j}(v^*) + d_{i,j}(v^*) = 0 \tag{10}$$

holds for all $j = p, \ldots, i-1$.

We remark that the high-level controller (6) associated with properties P1–P3 provides guidelines for designing either linear or nonlinear connected car-following dynamics.

Theorem 1: If vehicles $p, \ldots, i-1$ are in the uniform flow equilibrium (4), the connected car-following dynamics (2) and (6) with properties P1–P3 has a unique uniform flow equilibrium (5) that is independent of the network size, information delays, and connectivity topologies.

The proof is given in Appendix A. The uniqueness and independence of the uniform flow equilibrium are crucial for ensuring the performance of the CCC vehicle in real traffic environment.

Now, we seek for conditions that can guarantee the stability of the equilibrium (5). We define the perturbation about the equilibrium (5) as

$$\tilde{x}_{id}(t) = x_{id}(t) - x_{id}^*(t) = \begin{bmatrix} \tilde{s}_{id}(t) \\ \tilde{v}_{id}(t) \end{bmatrix}. \tag{11}$$

Note that perturbations of vehicles $p, \ldots, i-1$ will propagate backward along the vehicle chain and finally affect the motion of vehicle i. Thus, to enable vehicle i to approach the equilibrium, it is necessary that all vehicles ahead are in equilibrium, i.e., $x_j(t) = x_j^*(t)$ for all $t \geq 0$ and $j = p, \ldots, i-1$. This leads to

$$d_{i,j}(v_j(t-\xi_{i,j})) \equiv d_{i,j}(v^*) \tag{12}$$

in (6) for all j values. Substituting (4), (5), and (12) into the closed-loop system (2) and (6) and subtracting the result from (2) and (6), we obtain

$$\dot{\tilde{x}}_{id}(t) = \begin{bmatrix} \tilde{v}_{id}(t) \\ \sum_{j=p}^{i-1} \gamma_{i,j}\big(\tilde{f}_{i,j}(h_{id,j}) + \tilde{g}_{i,j}(v_{id})\big) \end{bmatrix} \tag{13}$$

where

$$\begin{aligned} \tilde{f}_{i,j}(h_{id,j}) &= f_{i,j}(h_{id,j}(t-\xi_{i,j})) - f_{i,j}\big(h_{id,j}^*\big) \\ \tilde{g}_{i,j}(v_{id}) &= g_{i,j}(v_{id}(t-\xi_{i,j})) - g_{i,j}(v^*). \end{aligned} \tag{14}$$

In practice, it is often desired that the distance and the velocity stay inside a given operating domain, that is

$$h_{id,i-1}(t) \in \mathcal{D}_h \subset \mathbb{R}_+, \quad v_{id}(t) \in \mathcal{D}_v \subset \mathbb{R}_+ \tag{15}$$

for all $t \geq 0$. We assume that the domains $\mathcal{D}_h$ and $\mathcal{D}_v$ are compact and the uniform flow equilibrium is inside the operating domain, i.e., $h_{j,j-1}^* \equiv h^* \in \mathcal{D}_h$ and $v_j^* \in \mathcal{D}_v$. When all vehicles $j = p, \ldots, i-1$ are in the equilibrium, it follows that:

$$h_{j,j-1}(t) \equiv h^* \in \mathcal{D}_h, \quad v_j(t) \equiv v^* \in \mathcal{D}_v. \tag{16}$$

According to (8), we can rewrite the average distance as

$$h_{id,j}(t) = \frac{1}{i-j}(h_{id,i-1}(t) + \cdots + h_{p+1,p}(t)). \tag{17}$$

Since all distances $h_{id,i-1}, \ldots, h_{p+1,p}$ are in the domain $\mathcal{D}_h$, the average distance $h_{id,j}$ is also in the domain $\mathcal{D}_h$. Considering this and (15), we have

$$h_{id,j}(t),\quad h^*_{id,j} \in \mathcal{D}_h,\ v^*_{id} \in \mathcal{D}_v \tag{18}$$

for $t \geq 0$ and all j values. Since $f_{i,j}(h)$ and $g_{i,j}(v)$ are differentiable with respect to h and v, respectively, based on the mean value theorem, there exist variables $\psi_{i,j} \in \mathcal{D}_h$ and $\varrho_{i,j} \in \mathcal{D}_v$, such that (14) can be written as

$$\begin{aligned}\tilde{f}_{i,j}(h_{id,j}) &= \frac{df_{i,j}(\psi_{i,j})}{dh_{id,j}}\big(h_{id,j}(t-\xi_{i,j}) - h^*_{id,j}\big)\\ &= -\frac{1}{i-j}\frac{df_{i,j}(\psi_{i,j})}{dh_{id,j}}\tilde{s}_{id}(t-\xi_{i,j})\\ \tilde{g}_{i,j}(v_{id}) &= \frac{dg_{i,j}(\varrho_{i,j})}{dv_{id}}\tilde{v}_{id}(t-\xi_{i,j})\end{aligned} \tag{19}$$

see (8) and (9). Note that the value of $\psi_{i,j}$ depends on $h_{id,j}(t-\xi_{i,j})$ and $h^*_{id,j}$ while the value of $\varrho_{i,j}$ is determined by $v_{id}(t-\xi_{i,j})$ and v^*. We remark that the expressions for $\psi_{i,j}$ and $\varrho_{i,j}$ are not needed, since the subsequent analysis only relies on their bounds $\mathcal{D}_h$ and $\mathcal{D}_v$.

Substituting (19) into (13) and writing the result into the matrix form, we obtain

$$\dot{\tilde{x}}_{id}(t) = A_{i,0}\tilde{x}_{id}(t) + \sum_{j=p}^{i-1} A_{i,j}(\Psi)\tilde{x}_{id}(t-\xi_{i,j}) \tag{20}$$

where $\Psi = [\psi_{i,p}, \ldots, \psi_{i,i-1}, \varrho_{i,p}, \ldots, \varrho_{i,i-1}] \in \mathcal{D}_h^{i-p} \times \mathcal{D}_v^{i-p}$ with the superscript "$i-p$" denoting the direct product of $\mathcal{D}_h$ or $\mathcal{D}_v$ with itself $i-p$ times. The matrices in (20) are given by

$$\begin{aligned}A_{i,0} &= \begin{bmatrix}0 & 1\\ 0 & 0\end{bmatrix}\\ A_{i,j}(\Psi) &= \gamma_{i,j}\begin{bmatrix}0 & 0\\ -\frac{1}{i-j}\frac{df_{i,j}(\psi_{i,j})}{dh_{id,j}} & \frac{dg_{i,j}(\varrho_{i,j})}{dv_{id}}\end{bmatrix}\end{aligned} \tag{21}$$

for $j = p, \ldots, i-1$. Note that every element in $A_{i,j}(\Psi)$ is bounded for all $\Psi \in \mathcal{D}_h^{i-p} \times \mathcal{D}_v^{i-p}$, since the functions $f_{i,j}(h)$ and $g_{i,j}(v)$ are continuously differentiable while $\psi_{i,j}$ and $\varrho_{i,j}$ belong to the compact sets $\mathcal{D}_h$ and $\mathcal{D}_v$, respectively.

Note that the information delays between different pairs of vehicles may have the same value, i.e., $\xi_{i,j} = \xi_{i,k}$ for $j \neq k$. To eliminate such redundancy, we define an ordered set $\sigma_i = \{\sigma_{i,0}, \sigma_{i,1}, \ldots, \sigma_{i,m}\}$ with $\sigma_{i,0} = 0$ and $\sigma_{i,j} < \sigma_{i,k}$ for $j < k$, which contains all delay values. Here, we include 0 as an element in the set σ_i to make the subsequent expressions more compact. Collecting terms in (20) according to the values of delays yields

$$\dot{\tilde{x}}_{id}(t) = \sum_{k=0}^{m} \hat{A}_{i,k}(\Psi)\tilde{x}_{id}(t-\sigma_{i,k}) \tag{22}$$

where $\hat{A}_{i,k}(\Psi)$ is the summation of $A_{i,j}(\Psi)$ that corresponds to the same value of delay. Indeed, the models (20) and (22) are equivalent but describe the system from different aspects. The model (20) emphasizes the connectivity topology of the network while (22) highlights distinct values of time delays.

Using the Newton–Leibniz formula yields the identity

$$\begin{aligned}\tilde{x}_{id}(t-\sigma_{i,k}) &= \tilde{x}_{id}(t) - \int_{t-\sigma_{i,k}}^{t}\dot{\tilde{x}}_{id}(\tau)d\tau\\ &= \tilde{x}_{id}(t) - \sum_{l=1}^{k}\int_{t-\sigma_{i,l}}^{t-\sigma_{i,l-1}}\dot{\tilde{x}}_{id}(\tau)d\tau.\end{aligned} \tag{23}$$

Substituting (23) into (22) leads to

$$\dot{\tilde{x}}_{id}(t) = \overline{A}_{i,0}(\Psi)\tilde{x}_{id}(t) - \sum_{q=1}^{m}\overline{A}_{i,q}(\Psi)\int_{t-\sigma_{i,q}}^{t-\sigma_{i,q-1}}\dot{\tilde{x}}_{id}(\tau)d\tau \tag{24}$$

where

$$\overline{A}_{i,q}(\Psi) = \sum_{k=q}^{m}\hat{A}_{i,k}(\Psi),\quad q = 0, \ldots, m. \tag{25}$$

In the remainder of this paper, we will not spell out the argument Ψ in $\hat{A}_{i,k}(\Psi)$ and $\overline{A}_{i,q}(\Psi)$ for simplicity. Based on (22) and (24), we present a delay-dependent condition, which ensures the asymptotic stability of the equilibrium of CCC dynamics (2) and (6).

Theorem 2: For the CCC dynamics (2) and (6) with properties P1–P3, the equilibrium (5) is asymptotically stable if the assumptions (15) and (16) hold and there exist positive definite matrices $P, Q_1, \ldots, Q_m, R_2, \ldots, R_m, W_1, \ldots, W_m \in \mathbb{R}^{2\times 2}$, such that the matrices

$$\begin{aligned}\Xi_1 &= \begin{bmatrix} Z & Y_{0,1} & \cdots & Y_{0,m} & -P\overline{A}_{i,1}\\ Y_{1,0} & Y_{1,1} - \frac{Q_1}{\sigma_{i,1}} & \cdots & Y_{1,m} & \mathbf{0}_{2\times 2}\\ \vdots & \vdots & \ddots & \vdots & \vdots\\ Y_{m,1} & Y_{m,2} & \cdots & Y_{m,m} - \frac{Q_m}{\sigma_{i,1}} & \mathbf{0}_{2\times 2}\\ -\overline{A}_{i,1}^T P & \mathbf{0}_{2\times 2} & \cdots & \mathbf{0}_{2\times 2} & -W_1\end{bmatrix}\\ \Xi_q &= \begin{bmatrix} -R_q & -P\overline{A}_{i,q}\\ -\overline{A}_{i,q}^T P & -W_q\end{bmatrix}\end{aligned} \tag{26}$$

are negative definite for all $q = 2, \ldots, m$ and for all $\Psi \in \mathcal{D}_h^{i-p} \times \mathcal{D}_v^{i-p}$. Here, $\mathbf{0}_{2\times 2}$ denotes the 2-by-2 zero matrix and other matrices are given by

$$\begin{aligned}Y_{j,k} &= \frac{\sum_{q=1}^{m}(\sigma_q - \sigma_{q-1})\hat{A}_{i,j}^T W_q \hat{A}_{i,k}}{\sigma_{i,1}}\\ Z &= \frac{1}{\sigma_{i,1}}\Bigg(P\overline{A}_{i,0} + \overline{A}_{i,0}^T P + \sum_{q=1}^{m} Q_q + \sigma_{i,1}Y_{0,0}\\ &\qquad + \sum_{q=2}^{m}(\sigma_{i,q} - \sigma_{i,q-1})R_q\Bigg).\end{aligned} \tag{27}$$

The proof of Theorem 2 is provided in Appendix B. We remark that the matrices $\Xi_1, \ldots, \Xi_m, Y_{j,k}, Z$ depend on the vehicle index i through $\hat{A}_{i,k}$ and $\overline{A}_{i,q}$ [see (26) and (27)], but this is not spelled out to keep the formulas more compact. Also note that Ξ_q depends on Ψ, for $q = 1, \ldots, m$; see (22), (24), and (26). To apply Theorem 2, we discretize the domain $\mathcal{D}_h^{i-p} \times \mathcal{D}_v^{i-p}$, which leads to n discrete points y_k for $k = 1, \ldots, n$. Then, we solve the linear matrix inequalities (LMIs) $\Xi_q(y_k) < 0$ for $q = 1, \ldots, m$ and $k = 1, \ldots, n$ for positive definite matrices $P, Q_1, \ldots, Q_m, R_2, \ldots, R_m, W_1, \ldots, W_m$ by using numerical LMI solvers. There may exist multiple solutions but we stop the calculation when one solution is found. Finally, we remark that Theorem 2 may not guarantee uniformly exponential stability defined in [22], where the perturbations converge to zero at the exponential speed.

We emphasize that the asymptotic stability of the equilibrium is a fundamental requirement for CCC design, since an unstable equilibrium would lead to safety problems, as shown in Fig. 5(c) and (d). In real traffic where the motion of vehicles varies in time, satisfying the conditions of Theorem 2 enables the CCC vehicle to follow the vehicles ahead. Based on Theorem 2, additional properties, such as disturbance attenuation, can be investigated, but these are outside the scope of this paper.

A specific high-level controller that satisfies the framework (6) with the corresponding properties was presented in [16], that is

$$u_{id}(t) = \sum_{j=p}^{i-1} \gamma_{i,j}[\alpha_{i,j}(V_i(h_{id,j}(t-\xi_{i,j})) - v_{id}(t-\xi_{i,j})) + \beta_{i,j}(v_j(t-\xi_{i,j}) - v_{id}(t-\xi_{i,j}))] \quad (28)$$

which corresponds to $f_{i,j}(h) = \alpha_{i,j} V_i(h)$, $d_{i,j}(v) = \beta_{i,j} v$, and $g_{i,j}(v) = -(\alpha_{i,j} + \beta_{i,j})v$. Here, the positive gain $\alpha_{i,j}$ corresponds to the distance $h_{id,j}$, and the positive gain $\beta_{i,j}$ corresponds to the relative velocity $v_j - v_{id}$, while the range policy function $V_i(h)$ determines the desired velocity based on the distance h. Here, we use the range policy

$$V_i(h) = \begin{cases} 0, & \text{if } h \le h_{\text{st},i} \\ \dfrac{v_{\max,i}}{2}\left[1 - \cos\left(\dfrac{\pi(h - h_{\text{st},i})}{h_{\text{go},i} - h_{\text{st},i}}\right)\right] & \text{if } h_{\text{st},i} < h < h_{\text{go},i} \\ v_{\max,i}, & \text{if } h \ge h_{\text{go},i}. \end{cases} \quad (29)$$

This indicates that the vehicle intends to stop for small distances $h \le h_{\text{st},i}$ while aiming to keep the preset maximum velocity $v_{\max,i}$ for large distances $h \ge h_{\text{go},i}$. In the middle range $h_{\text{st},i} < h < h_{\text{go},i}$, the desired velocity increases with the distance h. Notice that $V_i(h)$ is continuously differentiable for all h values, which can improve the ride comfort. Moreover, the function (29) is strictly monotonically increasing with respect to h in the operating domain $\mathcal{D}_h = \{h : h_{\text{st},i} < h < h_{\text{go},i}\}$ and $\mathcal{D}_v = \{v : 0 < v < v_{\max,i}\}$.

Based on Theorem 1, the high-level controller (28) ensures the existence of a unique uniform flow equilibrium. To guarantee the asymptotic stability of this equilibrium, the control gains $\alpha_{i,j}$ and $\beta_{i,j}$ should be designed to satisfy Theorem 2. Readers may refer to [16] for detailed calculation to find feasible values for $\alpha_{i,j}$ and $\beta_{i,j}$.

B. Low Level: Adaptive Sliding-Mode Control

The objective of the low-level controller is to regulate the axle torque, such that the vehicle state x_i tracks the desired state x_{id} generated by the high-level controller, that is

$$x_i(t) \to x_{id}(t), \quad \text{as} \quad t \to \infty. \quad (30)$$

In particular, we consider the physics-based vehicle model given in [14] and [23] and write (3) in the form

$$\begin{bmatrix} \dot{s}_i \\ \dot{v}_i \end{bmatrix} = \begin{bmatrix} v_i \\ -\dfrac{mg\sin\phi_i}{m_{\text{eff}}} - \dfrac{rmg\cos\phi_i}{m_{\text{eff}}} - \dfrac{k(v_i + v_{w,i})^2}{m_{\text{eff}}} + \dfrac{T_{a,i}}{m_{\text{eff}} R} \end{bmatrix} \quad (31)$$

see (1), where the effective mass $m_{\text{eff}} = m + J/R^2$ contains the vehicle mass m, the moment of inertia J of the rotating elements, and the wheel radius R. Moreover, g is the gravitational constant, r is the rolling resistance coefficient, and k is the aerodynamic drag constant. The external disturbances include the road angle ϕ_i and the headwind speed $v_{w,i}$. Here, we design a controller for the axle torque $T_{a,i} = \eta_i T_{\text{en},i}$, which is determined by the engine torque $T_{\text{en},i}$ and the constant η_i = gear ratio × final drive ratio; see Appendix D for specific parameters of a heavy-duty vehicle. We assume that the onboard sensors are able to measure the states sufficiently fast, so that the corresponding time delays can be neglected. Thus, we dropped the argument t in (31) to make the expressions more compact.

Multiplying the second equation in (31) by $m_{\text{eff}} R$ yields

$$\theta_{i,1}\dot{v}_i = -\theta_{i,2}\sin\phi_i - \theta_{i,3}\cos\phi_i - \theta_{i,4}(v_i + v_{w,i})^2 + T_{a,i} \quad (32)$$

where

$$\theta_{i,1} = m_{\text{eff}} R, \quad \theta_{i,2} = mgR, \quad \theta_{i,3} = rmgR, \quad \theta_{i,4} = kR. \quad (33)$$

For compactness, we use $\theta_i = [\theta_{i,1}, \theta_{i,2}, \theta_{i,3}, \theta_{i,4}]^T$.

Considering the estimated vehicle parameters

$$\hat{\theta}_i = [\hat{\theta}_{i,1}, \hat{\theta}_{i,2}, \hat{\theta}_{i,3}, \hat{\theta}_{i,4}]^T \quad (34)$$

and assuming the estimated headwind speed $\hat{v}_{w,i}$, one can design the low-level controller in the form

$$T_{a,i} = \hat{\theta}_{i,1} u_i + \hat{\theta}_{i,2}\sin\phi_i + \hat{\theta}_{i,3}\cos\phi_i + \hat{\theta}_{i,4}(v_i + \hat{v}_{w,i})^2 \quad (35)$$

where u_i is given by the high-level controller (6) but replacing the desired state x_{id} with the actual state x_i. Indeed, the controller (35) is designed by incorporating the desired dynamics (2) and (6) while trying to cancel the nonlinear terms in (32) by using the feedback signals. When the estimated values of parameters and headwind speed match the real ones, i.e., $\theta_i = \hat{\theta}_i$ and $v_{w,i} = \hat{v}_{w,i}$, the closed-loop dynamics (31) and (35) indeed become the desired dynamics (2) and (6).

However, in practice, vehicle parameters may be not exactly known while the headwind speed varies in time. Hence, the controller (35) may not ensure the required tracking performance. Thus, we seek for controllers that can guarantee tracking performance while remaining robust against uncertainties in parameters and external disturbances. Here, we assume that the vehicle parameters and the headwind speed are bounded with known bounds. In particular, we denote

$$k \leq \overline{k}, \quad R \leq \overline{R}, \quad \underline{v}_w \leq v_{w,i} \leq \overline{v}_w \tag{36}$$

where $\overline{k}$, $\overline{R}$, $\underline{v}_w$, and $\overline{v}_w$ are all constants. It follows that

$$\theta_{i,4} \leq \overline{kR} \tag{37}$$

see (33). We write the headwind speed in the form

$$v_{w,i} = \overline{\overline{v}}_w + \tilde{v}_{w,i} \tag{38}$$

where the first term is a constant denoting the average speed

$$\overline{\overline{v}}_w = \frac{\underline{v}_w + \overline{v}_w}{2} \tag{39}$$

while the second term denotes the uncertainty bounded as

$$|\tilde{v}_{w,i}| \leq \frac{\overline{v}_w - \underline{v}_w}{2}. \tag{40}$$

Substituting (38) into (32) yields

$$\begin{aligned}\theta_{i,1}\dot{v}_i &= -\theta_{i,2}\sin\phi_i - \theta_{i,3}\cos\phi_i - \theta_{i,4}(v_i + \overline{\overline{v}}_w)^2 \\ &\quad + \delta(v_i, \tilde{v}_{w,i}) + T_{a,i}\end{aligned} \tag{41}$$

where the uncertain disturbance is given by

$$\delta(v_i, \tilde{v}_{w,i}) = -\theta_{i,4}\big(2\tilde{v}_{w,i}(v_i + \overline{\overline{v}}_w) + \tilde{v}_{w,i}^2\big). \tag{42}$$

Considering the bounds (37) and (40), one can obtain the upper bound of the unknown disturbance

$$\begin{aligned}|\delta(v_i, \tilde{v}_{w,i})| &\leq \overline{kR}\left((\overline{v}_w - \underline{v}_w)(v_i + \overline{\overline{v}}_w) + \left(\frac{\overline{v}_w - \underline{v}_w}{2}\right)^2\right) \\ &\triangleq \overline{\delta}(v_i)\end{aligned} \tag{43}$$

which depends on the vehicle speed v_i.

We assume that the vehicle state x_i and the inclination angle ϕ_i can be obtained via onboard sensors, digital maps, and global positioning system. To enable the vehicle to track the desired dynamics while counteracting the uncertain vehicle dynamics, one may use sliding-mode control [24]. However, this method may lead to conservative results, since it relies on the upper bounds of uncertainties for robustness. Here, we combine sliding-mode control with adaptive control [25]. In particular, adaptive control is used to adjust to the uncertain constant parameters and sliding-mode control is applied to compensate for the time-varying disturbances. We remark that the combination of these two methods ensures fast tracking and also reduces the conservativeness.

To design the low-level controller, we first define a sliding surface

$$S_i \triangleq v_i - v_{id} + \lambda_1(s_i - s_{id}) = 0 \tag{44}$$

where s_{id} and v_{id} are the desired states given by the high-level controller while λ_1 is a positive parameter. Since $\dot{s}_i = v_i$ and $\dot{s}_{id} = v_{id}$, the system approaches $s_i = s_{id}$ and $v_i = v_{id}$ when it travels along the sliding surface (44). Then, we design a controller that regulates the state to reach the sliding surface. Based on (43) and (44), we propose the controller for the axle torque

$$T_{a,i} = \hat{\theta}_i^T w - \overline{\delta}(v_i)\mathrm{sgn}(S_i) - \lambda_2 S_i \tag{45}$$

where the parameter estimate $\hat{\theta}_i$ is given in (34), the positive constant λ_2 is a tuning parameter, and the vector w is constructed as

$$w = \begin{bmatrix} w_1 \\ w_2 \\ w_3 \\ w_4 \end{bmatrix} = \begin{bmatrix} \dot{v}_{id} - \lambda_1(v_i - v_{id}) \\ \sin\phi_i \\ \cos\phi_i \\ (v_i + \hat{v}_w)^2 \end{bmatrix}. \tag{46}$$

The adaptation law for the estimate $\hat{\theta}_i$ is given by

$$\dot{\hat{\theta}}_i = -S_i \Gamma w \tag{47}$$

where the positive definite matrix $\Gamma \in \mathbb{R}^{4\times 4}$ contains the adaptation gains. In the controller (45), the first and the second terms are used to counteract the uncertainties arising from constant parameters and time-varying disturbances, respectively, and the third term is used to push the system toward the sliding surface (44).

Theorem 3: If the modeling uncertainties have known bounds (36), the low-level controller (44)–(47) guarantees that the vehicle dynamics (31) track the desired motion generated by the high-level controller in the sense of (30).

The proof is given in Appendix C. In the low-level controller (44)–(47), λ_1 determines the decaying speed of tracking errors along the sliding surface $S_i = 0$ while λ_2 determines the speed for approaching the sliding surface. In practice, λ_2 shall be a large number, since the effective gain on the acceleration for the closed-loop system (32) and (45) is indeed $\lambda_2/\theta_{i,1}$ and $\theta_{i,1}$ is a large number; see (33).

In the adaptation law (47), we use a diagonal matrix $\Gamma = \mathrm{diag}\{\Gamma_1, \Gamma_2, \Gamma_3, \Gamma_4\}$, where $\Gamma_1, \ldots, \Gamma_4$ are all positive scalars. Note that the adaptation speed of $\hat{\theta}_{i,k}$ is proportional to $\Gamma_k w_k$ for $k = 1, \ldots, 4$. In practice, the inclination angle ϕ_i is small, yielding $w_2 \approx 0$. In this case, Γ_2 has little influence on the adaptation. Considering that the value of w_4 may be much larger than the values of w_1, w_2, and w_3, one may choose Γ_4 to be a small number. Note that, in general, the adaptation law (47) may not regulate $\hat{\theta}_i$ to approach the actual value θ_i, since the excitation becomes weak when the state is around the sliding surface, i.e., $S_i \approx 0$. However, this does not affect the tracking performance, as will be demonstrated by numerical simulations in Section III.

The parameters in the controller (44)–(47) should be appropriately designed to achieve fast tracking while avoiding transient oscillations. For different problems, the range of feasible parameters may vary. The tuning of these parameters is typically done through analysis and simulation, as will be shown in our case study in Section III.

When implementing the controller (45), the discontinuities of the term $\mathrm{sgn}(S_i)$ may cause undesired chattering around the sliding surface (44). In practice, we replace the term $\mathrm{sgn}(S_i)$ by a continuous saturation function

$$\mathrm{sat}(S_i/\Phi_i) = \begin{cases} S_i/\Phi_i, & \text{if } |S_i| \leq \Phi_i \\ \mathrm{sgn}(S_i), & \text{otherwise} \end{cases} \tag{48}$$

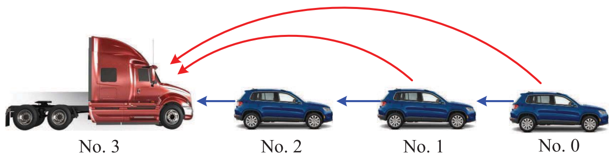

Fig. 3. (3+1)-vehicle network where vehicle 3 is a heavy-duty truck equipped with CCC. The other vehicles are human-driven vehicles that only respond to the motion of the vehicle immediately ahead.

where the positive constant Φ_i defines the boundary layer that is an invariant region around the sliding surface. Note that large values of Φ_i may deteriorate the tracking performance while small values of Φ_i may still lead to chattering phenomenon. Thus, in practice, Φ_i should be chosen by considering the tradeoff between the tracking performance and the chattering avoidance.

Combining the high-level controller (2) and (6) and the low-level controller (44)–(47) results in a CCC which contains eight states ($x_{id} \in \mathbb{R}^2$, $x_i \in \mathbb{R}^2$, $\hat{\theta}_i \in \mathbb{R}^4$) and is excited by $2(i-p)$ inputs $[x_{i-1}, \ldots, x_p$ in (6)] as well as two external disturbances [ϕ_i and $v_{w,i}$ in (31)].

III. Case Study and Simulations

In this section, we apply the CCC presented in Section II to a heavy-duty vehicle in a $(3+1)$-vehicle network shown in Fig. 3. Numerical simulations are conducted by using MATLAB to validate the analytical results and test the performance of the system. The differential equations are solved by applying the explicit Euler method with time step 0.1 [s].

In Fig. 3, heavy-duty vehicle 3 is equipped with CCC while human-driven vehicles 0–2 only respond to the motion of the vehicle immediately ahead. We consider that vehicle 3 receives motion data from vehicles 0 and 1 with delays $\xi_{3,0} = \xi_{3,1} = 0.2$ [s], which are caused by intermittency and packet drops in the wireless communication. We also consider the scenario where vehicle 3 is driven by a human driver who monitors the motion of vehicle 2 with reaction delay $\xi_{3,2} = 0.5$ [s] while the CCC is used to assist the driver. We assume that the parameters in range policy (29) are $h_{\mathrm{st},3} = 5$ [m], $h_{\mathrm{go},3} = 35$ [m], and $v_{\max,3} = 30$ [m/s]. The parameters of the heavy-duty truck are provided in Appendix D while the gear shift map is shown in Fig. 4(a), where the blue and the red curves represent the upshift and the downshift, respectively; see [26].

We assume that the head vehicle 0 has length $l_0 = 4.8$ [m] while its velocity is given by experimental data collected through the UMTRI Safety Pilot Project [27], where the speed is measured every 0.1 [s]. The speed profile of vehicle 0 is shown in Fig. 4(b). The connected car-following dynamics of vehicles $j = 1, 2$ are modeled using (2), (28), and (29) where $\gamma_{j,j-1} = 1$ but $\gamma_{j,k} = 0$ for all $k \neq j-1$. The parameters of vehicles $j = 1, 2$ are set as follows.

1) $l_1 = 4.5$ [m], $\alpha_{1,0} = 0.5$ [1/s], $\beta_{1,0} = 0.7$ [1/s], $h_{\mathrm{st},1} = 3$ [m], $h_{\mathrm{go},1} = 40$ [m], $v_{\max,1} = 30$ [m/s], and $\xi_{1,0} = 0.8$ [s].
2) $l_2 = 4$ [m], $\alpha_{2,1} = 0.3$ [1/s], $\beta_{2,1} = 0.6$ [1/s], $h_{\mathrm{st},2} = 4$ [m], $h_{\mathrm{go},2} = 38$ [m], $v_{\max,2} = 32$ [m/s], and $\xi_{2,1} = 0.6$ [s].

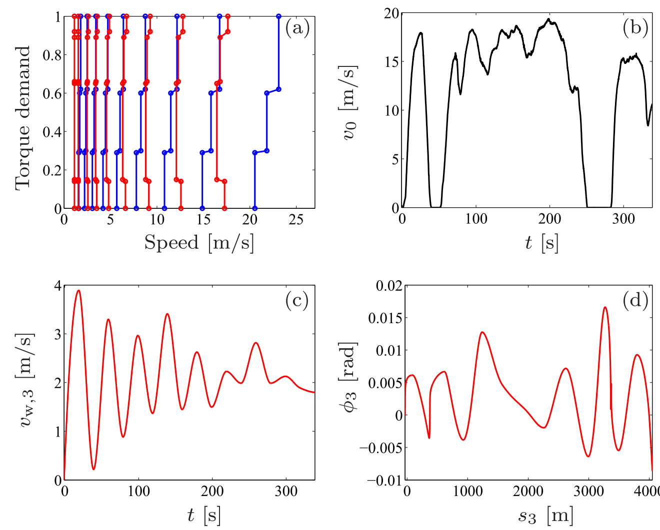

Fig. 4. (a) Gear shift map for the heavy-duty vehicle, where the blue and the red curves indicate upshift and downshift, respectively. (b) Velocity profile of vehicle 0. (c) and (d) Headwind speed and road inclination angle.

For the headwind speed $v_{w,3}$, we assume that it can be modeled by an autoregressive moving average model [28]. Here, we use

$$v_{w,3}(t_k) = -c_1 v_{w,3}(t_{k-1}) + \rho + e_1 \epsilon(t_k) \tag{49}$$

where $t_k = t_{k-1} + 20$ [s] for $k = 1, 2, \ldots$, ϵ is a random variable between 0 and 1, and c_1, ρ, and e_1 are constants. Here, we use $c_1 = 0.9$, $\rho = 3$ [m/s], and $e_1 = 1.8$ [m/s]. For the road angle, we also assume the form (49) while replacing $v_{w,3}$ by ϕ_3. The corresponding parameters are set to be $c_1 = 0.3$, $\rho = 0$ [deg], and $e_1 = 0.4$ [deg]. For simulation, we interpolate between points of the headwind speed and the road angle, leading to the trajectories displayed in Fig. 4(c) and (d), respectively.

When designing CCC for vehicle 3, we use the hierarchical framework presented in Section II. For the high-level controller, we use (28) with control gains $\alpha_{3,2} = 0.3$ [1/s], $\beta_{3,2} = 0.5$ [1/s], $\alpha_{3,1} = 0$ [1/s], $\beta_{3,1} = 1$ [1/s], $\alpha_{3,0} = 0.2$ [1/s], and $\beta_{3,0} = 0.2$ [1/s]. This set of parameters are obtained by satisfying Theorem 2, and the detailed calculation is given in [16]. When vehicles 0–2 are in the uniform flow equilibrium, this set of parameters enable vehicle 3 to approach the equilibrium. Moreover, if vehicles 0–2 are not in the equilibrium, this set of parameters leads to stable CCC dynamics, as shown in Fig. 5(a) and (b). If Theorem 2 was not satisfied, the CCC dynamics could become unstable and the perturbations about the trajectory diverge, as displayed in Fig. 5(c) and (d). In particular, Fig. 5(c) shows that the distances are negative in some time intervals, implying that unstable dynamics lead to collisions.

For the low-level controller, we first use the controller (35) as the benchmark. When the estimated parameter values and headwind speed exactly match their real values, this controller leads to $s_3(t) = s_{3d}(t)$ and $v_3(t) = v_{3d}(t)$ for all $t \geq 0$. Now, we consider estimated values $\hat{m} = 30\,000$ [kg], $\hat{k} = 7.7$ [kg/m], $\hat{r} = 0.01$, and $\hat{R} = 0.6$ [m], which are different from the actual values given in Appendix D.

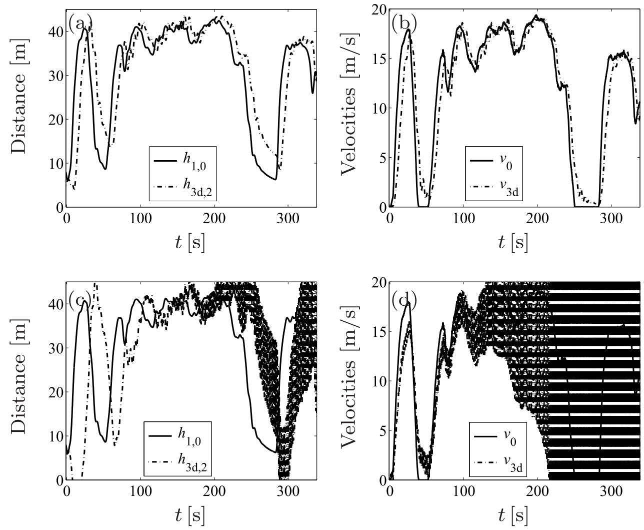

Fig. 5. (a) and (b) Stable connected car-following dynamics: perturbations about the trajectory decay to zero when Theorem 2 is satisfied. (c) and (d) Unstable connected car-following dynamics: perturbations about the trajectory may diverge when Theorem 2 is not satisfied.

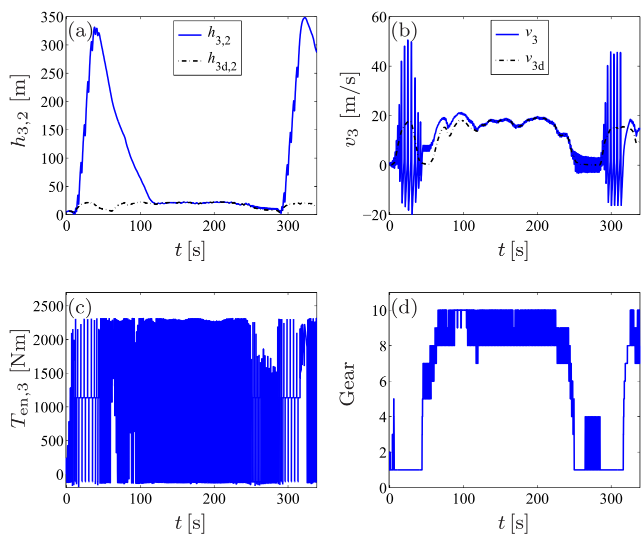

Fig. 6. Simulation results when the high-level controller (28) is applied with the low-level controller (35). (a) and (b) Distance $h_{3,2}$ and velocity v_3 of vehicle 3, where the dashed dotted curves denote the desired state given by the high-level controller while the blue solid curves are for the vehicle state regulated by the low-level controller. (c) and (d) Engine torque $T_{en,3}$ and gear shifts of vehicle 3.

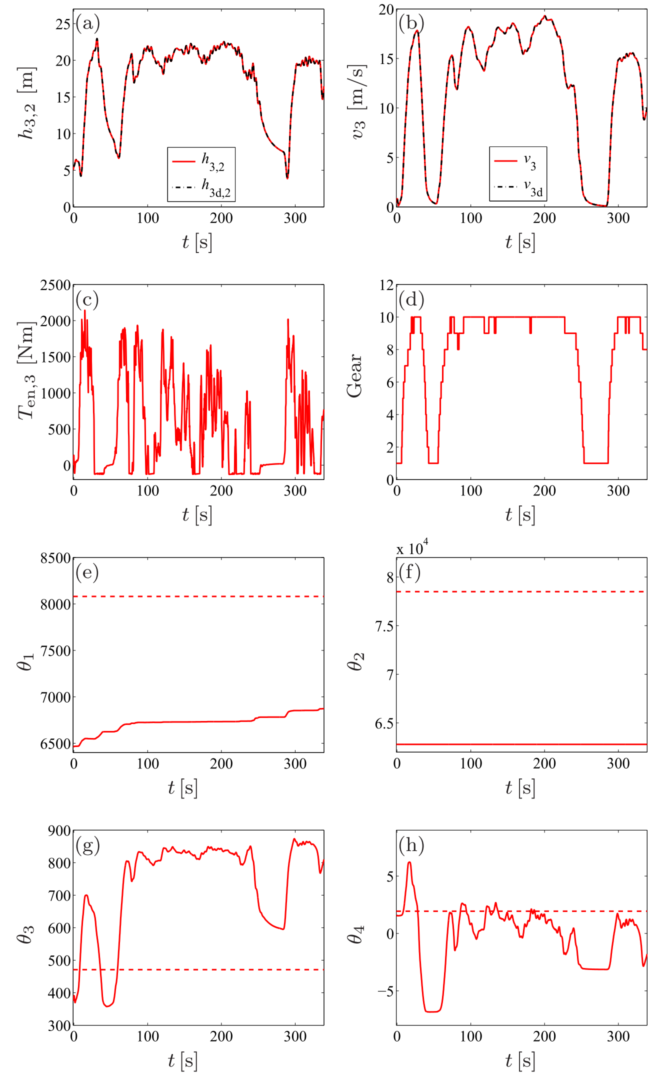

Fig. 7. Simulation results when the high-level controller (28) is applied with the adaptive sliding-mode controller (44)–(47). (a) and (b) Distance $h_{3,2}$ and velocity v_3 of vehicle 3. (c) and (d) Engine torque $T_{en,3}$ and gear shifts of vehicle 3. (e)–(h) Real vehicle parameters (dashed lines) and their estimates (solid curves).

The corresponding simulation results are shown in Fig. 6. The trajectories displayed in Fig. 6(a) and (b) show that the vehicle state (blue solid lines) cannot track the desired state (black dashed dotted lines) given by the high-level controller. Moreover, high-frequency oscillations are generated in the engine torque and gear shifts, as displayed in Fig. 6(c) and (d). This may cause severe damage to the engine and the transmission.

Then, we apply the adaptive sliding-mode controller (44)–(47) as the low-level controller. In order to find feasible parameters to achieve fast tracking and avoid transient oscillations, we conducted a large number of simulations. Here, we summarize the range of feasible parameters as follows. The values of λ_1 and λ_2 can be selected in the ranges 0.1–10 and 10^4–10^5, respectively. The adaptation gains Γ_1 and Γ_3 should be selected in the range 10^2–10^3 while Γ_4 can be chosen between 0.1 and 1. Since Γ_2 has little impact on the parameter adaption, one can simply choose a value between 0 and 1. Here, we set the values to be $\lambda_1 = 1$ [1/s] and $\lambda_2 = 3 \times 10^4$ [kg·m/s] while the adaptation gains are given by $\Gamma = diag\{100, 1, 500, 0.1\}$ with units [kg·s/m], [N], [N], [kg·s^2/m^3], respectively. Moreover, the boundary layer in (48) is set to be $\Phi = 0.1$ [m/s]. The corresponding simulation results are displayed in Fig. 7. As shown in Fig. 7(a) and (b), the vehicle state (red solid lines) tracks the desired state (black dashed dotted lines) generated by the high-level controller. Fig. 7(c) and (d) shows the engine torque and the gear shifts with no high-frequency oscillations present. Comparing Figs. 6(c) and 7(c), one may also observe the advantage of the adaptive sliding-mode controller in leading to realistic torque inputs. Fig. 7(e)–(h) shows that the parameter estimates do not converge to the real value, but this does not affect the state tracking performance as shown in Fig. 7(a) and (b).

In summary, comparing the simulation result for benchmark controller (35) [blue curves in Fig. 6(a)–(d)] and that for adaptive sliding-mode controller [red curves in Fig. 7(a)–(d)], one can observe that the latter one can regulate the vehicle to track the desired state while counteracting uncertainties arising from parameters and external disturbances. Moreover, the adaptive sliding-mode controller improves the actuator performance by avoiding high-frequency oscillations.

IV. Conclusion

In this paper, we investigated CCC by incorporating the motion data received from multiple distant vehicles ahead via wireless V2V communication. To reduce the complexity of CCC design, we used a hierarchical framework. The high-level controller was designed to generate the connected car-following dynamics by exploiting the information received from multiple vehicles ahead. At the low level, we considered a physics-based vehicle model and designed an adaptive sliding-mode controller, which regulated the engine torque, such that the vehicle tracked the desired state in the presence of uncertain vehicle dynamics. Numerical simulations were used to validate the analytical results, which showed the advantage of the adaptive sliding-mode controller in tracking states and avoiding high-frequency oscillations.

System-level properties, such as disturbance attenuation and fuel efficiency, were not investigated. In the future, we will investigate the optimization of high-level controller to improve the system-level performance by exploiting V2V communication. Moreover, in practice, the information delays may be time-varying due to the stochastic packet drops in the communication [29]. How to enhance the robustness of our proposed general high-level controller against stochastic delays will be investigated in the future. For the design of the low-level controller, the input saturations on engine torque will also be considered in the future work.

Appendix A
Proof of Theorem 1

In system (2) and (6), we use the distance $h_{id,i-1}$ to replace the position s_{id} and obtain

$$\begin{aligned}\dot{h}_{id,i-1}(t) &= v_{i-1}(t) - v_{id}(t)\\ \dot{v}_{id}(t) &= \sum_{j=p}^{i-1}\gamma_{i,j}(f_{i,j}(h_{id,j}(t-\xi_{i,j})) + g_{i,j}(v_{id}(t-\xi_{i,j}))\\ &\qquad + d_{i,j}(v_j(t-\xi_{i,j}))).\end{aligned} \tag{50}$$

To investigate the equilibrium of vehicle i, we assume that vehicles $j = p, \ldots, i-1$ are in the uniform flow equilibrium, such that $h_{j,j-1}(t) = s^*_{j-1}(t) - s^*_j(t) - l_{j-1} \equiv h^*$ and $v_j(t) \equiv v^*$. This leads to

$$h^*_{id,j}(t) = \frac{h^*_{id,i-1}(t) + (i-j-1)h^*}{i-j} \tag{51}$$

see (9). Then, to solve the equilibrium of vehicle i, we set the derivatives to be zero, yielding

$$\begin{aligned}0 &= v^* - v^*_{id}(t)\\ 0 &= \sum_{j=p}^{i-1}\gamma_{i,j}\big(f_{i,j}\big(h^*_{id,j}(t-\xi_{i,j})\big) + g_{i,j}\big(v^*_{id}(t-\xi_{i,j})\big)\\ &\qquad + d_{i,j}(v^*)\big).\end{aligned} \tag{52}$$

The first equation leads to the equilibrium

$$v^*_{id}(t) \equiv v^*. \tag{53}$$

Substituting this into the second equation in (52) yields

$$0 = \sum_{j=p}^{i-1}\gamma_{i,j}\big(f_{i,j}\big(h^*_{id,j}(t-\xi_{i,j})\big) + g_{i,j}(v^*) + d_{i,j}(v^*)\big). \tag{54}$$

The property (10) ensures that $h^*_{id,j}(t) \equiv h^*$ is a solution of (54), which leads to

$$h^*_{id,i-1}(t) = s^*_{i-1}(t) - s^*_{id}(t) - l_{i-1} \equiv h^* \tag{55}$$

see (9). Based on (51), (54) can be written as

$$\begin{aligned}&\sum_{j=p}^{i-1}\gamma_{i,j} f_{i,j}\left(\frac{h^*_{id,i-1}(t) + (i-j-1)h^*}{i-j}\right)\\ &\qquad = -\sum_{j=p}^{i-1}\gamma_{i,j}(g_{i,j}(v^*) + d_{i,j}(v^*)).\end{aligned} \tag{56}$$

Since $f_{i,j}(h)$ must be strictly monotonically increasing functions with respect to h for all $j = p, \ldots, i-1$, the left-hand side of (56) is also a strictly monotonically increasing function with respect to $h^*_{id,i-1}(t)$, while the right-hand side is a constant. Thus, if there exists a solution for (56), then that solution is unique. Therefore, (55) is the unique solution of the equation (56). Based on (53) and (55), one can conclude that (5) is the unique equilibrium of the connected car-following dynamics (2) and (6).

Appendix B
Proof of Theorem 2

The asymptotic stability of the equilibrium (5) is equivalent to $\tilde{x}_{id}(t) = 0$ in (22) and (24), which is asymptotically stable. To prove $\tilde{x}_{id}(t) \to 0$ as $t \to \infty$, we use the Lyapunov–Krasovskii theorem with the functional

$$\begin{aligned}L &= \tilde{x}^T_{id}(t)P\tilde{x}_{id}(t) + \sum_{j=1}^{m}\int_{t-\sigma_{i,j}}^{t}\tilde{x}^T_{id}(\tau)Q_j\tilde{x}_{id}(\tau)d\tau\\ &\quad + \sum_{j=1}^{m}\int_{-\sigma_{i,j}}^{-\sigma_{i,j-1}}\int_{t+\theta}^{t}\dot{\tilde{x}}^T_{id}(\tau)W_j\dot{\tilde{x}}_{id}(\tau)d\tau d\theta\end{aligned} \tag{57}$$

where the matrices P, Q_j, and W_j are positive definite for $j = 1, \ldots, m$. Since the integration does not change the positive sign, it follows that L is positive definite.

Substituting (22) and (24) into the time derivative of (57) and adding the identity

$$0 = \sum_{q=2}^{m} (\sigma_{i,q} - \sigma_{i,q-1}) \tilde{x}_{id}^T(t) R_q \tilde{x}_{id}(t) - \sum_{q=2}^{m} \int_{t-\sigma_{i,q}}^{t-\sigma_{i,q-1}} \tilde{x}_{id}^T(t) R_q \tilde{x}_{id}(t) d\tau \tag{58}$$

yields

$$\begin{aligned}\dot{L} &= \Delta(t) - \sum_{j=1}^{m} 2\tilde{x}_{id}^T(t) P \overline{A}_{i,j} \int_{t-\sigma_{i,j}}^{t-\sigma_{i,j-1}} \dot{\tilde{x}}_{id}(\tau) d\tau \\ &\quad - \sum_{j=1}^{m} \int_{t-\sigma_{i,j}}^{t-\sigma_{i,j-1}} \dot{\tilde{x}}_{id}^T(\tau) W_j \dot{\tilde{x}}_{id}(\tau) d\tau \\ &\quad - \sum_{q=2}^{m} \int_{t-\sigma_{i,j}}^{t-\sigma_{i,j-1}} \tilde{x}_{id}^T(t) R_q \tilde{x}_{id}(t) d\tau \end{aligned} \tag{59}$$

where

$$\begin{aligned}\Delta(t) &= \sigma_{i,1} \tilde{x}_{id}^T(t)(Z - Y_{0,0})\tilde{x}_{id}(t) \\ &\quad - \sum_{j=1}^{m} \tilde{x}_{id}^T(t - \sigma_{i,j}) Q_j \tilde{x}_{id}(t - \sigma_{i,j}) \\ &\quad + E^T \left(\sum_{j=1}^{m} (\sigma_{i,j} - \sigma_{i,j-1}) W_j \right) E \end{aligned} \tag{60}$$

with $Y_{0,0}$ and Z given in (27) and

$$E = \sum_{k=0}^{m} \hat{A}_{i,k} \tilde{x}_{id}(t - \sigma_{i,k}). \tag{61}$$

Then, substituting the identity

$$\Delta(t) = \frac{1}{\sigma_{i,1}} \int_{t-\sigma_{i,1}}^{t} \Delta(t) d\tau \tag{62}$$

into (59) while writing the result in matrix form, we obtain

$$\begin{aligned}\dot{L} &= \int_{t-\sigma_{i,1}}^{t} \tilde{\chi}_i^T(t,\tau) \Xi_1 \tilde{\chi}_i(t,\tau) d\tau \\ &\quad + \sum_{q=2}^{m} \int_{t-\sigma_{i,q}}^{t-\sigma_{i,q-1}} \tilde{X}_i^T(t,\tau) \Xi_q \tilde{X}_i(t,\tau) d\tau \end{aligned} \tag{63}$$

where Ξ_j for $j = 1, \ldots, m$ are given in (26) and

$$\begin{aligned}\tilde{\chi}_i^T(t,\tau) &= \left[\tilde{x}_{id}^T(t - \sigma_{i,0}), \ldots, \tilde{x}_{id}^T(t - \sigma_{i,m_i}), \dot{\tilde{x}}_{id}^T(\tau)\right] \\ \tilde{X}_i^T(t,\tau) &= \left[\tilde{x}_{id}^T(t), \dot{\tilde{x}}_{id}^T(\tau)\right]. \end{aligned} \tag{64}$$

If Ξ_j are negative definite for $\forall \Psi \in \mathcal{D}_h^{i-p} \times \mathcal{D}_v^{i-p}$ and all $j = 1, \ldots, m$, the negative definiteness of $\dot{L}$ is guaranteed, since integration does not change the sign. This leads to $\tilde{x}_i(t) \to 0$ as $t \to \infty$ when the distance and the velocity stay inside the operating domain $\mathcal{D}_h$ and $\mathcal{D}_v$.

Appendix C
Proof of Theorem 3

To prove the asymptotically tracking, we use the Lyapunov function

$$L = \frac{\theta_{i,1}}{2} S_i^2 + \frac{1}{2} \tilde{\theta}_i^T \Gamma^{-1} \tilde{\theta}_i \tag{65}$$

where $\theta_{i,1}$, S_i, and Γ are given in (44), (33), and (47), respectively, while $\tilde{\theta}_i = \hat{\theta}_i - \theta_i$ denotes the difference between the estimate $\hat{\theta}_i$ and the real value θ_i.

Differentiating (65) with respect to time yields

$$\dot{L} = \theta_{i,1} \dot{S}_i S_i + \tilde{\theta}_i^T \Gamma^{-1} \dot{\hat{\theta}}_i. \tag{66}$$

Based on (41) and (44), we obtain

$$\begin{aligned}\theta_{i,1} \dot{S}_i &= \theta_{i,1} \dot{v}_i - \theta_{i,1}(\dot{v}_{id} - \lambda_1(v_i - v_{id})) \\ &= -\theta_i^T w + \delta(v_i, \tilde{v}_{w,i}) + T_{a,i} \end{aligned} \tag{67}$$

where the disturbance $\delta(v_i, \tilde{v}_{w,i})$ and the vector w are given in (42) and (46), respectively.

Substituting the controller (45) into (67) yields

$$\theta_{i,1} \dot{S}_i = \tilde{\theta}_i^T w + \delta(v_i, \tilde{v}_{w,i}) - \overline{\delta}(v_i)\mathrm{sgn}(S_i) - \lambda_2 S_i. \tag{68}$$

Substituting this into (66) yields

$$\begin{aligned}\dot{L} &= S_i \tilde{\theta}_i^T w + S_i \delta(v_i, \tilde{v}_{w,i}) - S_i \overline{\delta}(v_i)\mathrm{sgn}(S_i) \\ &\quad - \lambda_2 S_i^2 + \tilde{\theta}_i^T \Gamma^{-1} \dot{\hat{\theta}}_i \\ &= \tilde{\theta}_i^T \left(S_i w + \Gamma^{-1} \dot{\hat{\theta}}_i\right) + S_i \delta(v_i, \tilde{v}_{w,i}) \\ &\quad - S_i \overline{\delta}(v_i)\mathrm{sgn}(S_i) - \lambda_2 S_i^2. \end{aligned} \tag{69}$$

Considering the adaptation law (47) in (69), we obtain

$$\begin{aligned}\dot{L} &= S_i \delta(v_i, \tilde{v}_{w,i}) - |S_i| \overline{\delta}(v_i) - \lambda_2 S_i^2 \\ &\le |S_i|(|\delta(v_i, \tilde{v}_{w,i})| - \overline{\delta}(v_i)) - \lambda_2 S_i^2 \\ &\le -\lambda_2 S_i^2 \end{aligned} \tag{70}$$

see (43). Since $\dot{L}$ is negative semidefinite, it follows that $L(t) \le L(0)$, so that S_i and $\tilde{\theta}_i$ are bounded, which implies that the difference between the desired state and the real state $x_{id} - x_i$ is always bounded.

Consider the worst case scenario when $\delta(v_i, \tilde{v}_{w,i}) = \mathrm{sgn}(S_i)\overline{\delta}(v_i)$, which corresponds to the least decaying speed

$$\dot{L} = -\lambda_2 S_i^2 \tag{71}$$

see (70). Differentiating (71) with respect to time while considering (41) yields

$$\ddot{L} = -\frac{2\lambda_2}{\theta_{i,1}} S_i \left(\tilde{\theta}_i^T w + \delta(v_i, \tilde{v}_{w,i}) - \overline{\delta}(v_i)\mathrm{sgn}(S_i) - \lambda_2 S_i\right). \tag{72}$$

In practice, the vehicle speed v_i and the inclination angle ϕ_i are both bounded. Thus, the vector w is also bounded, which implies that $\ddot{L}$ is always bounded. This ensures that $\dot{L}$ is uniformly continuous. Since L is positive definite while $\dot{L}$ is seminegative definite and also uniformly continuous, based on Barbalet's lemma [30], we have $\dot{L} \to 0$, i.e., $S_i \to 0$, as $t \to \infty$; see (71). For nonworst case scenarios, we have $\dot{L} < -\lambda_2 \ S_i^2$ when $S_i \neq 0$, and thus, L decays at a faster speed until $S_i = 0$. At the sliding surface $S_i = 0$, we have $s_i \to s_{id}$ and $v_i \to v_{id}$ as $t \to \infty$; see (44).

TABLE I
PHYSICAL VEHICLE PARAMETERS

Parameter	Value
Mass (m)	15876 [kg]
Air Drag Coefficient (k)	3.8448 [kg/m]
Tire Rolling Radius (R)	0.5040 [m]
Tire Rolling Resistance Coefficient (r)	0.006
Engine Rotational Inertia (J)	5 $[\mathrm{kg}\cdot\mathrm{m}^2]$
Gravitational Constant (g)	9.81 $[\mathrm{m/s}^2]$
Maximum Engine Torque	2314.3 $[\mathrm{N}\cdot\mathrm{m}]$
Number of Forward Gears	10
1st Gear Ratio	12.94
2nd Gear Ratio	9.29
3rd Gear Ratio	6.75
4th Gear Ratio	4.90
5th Gear Ratio	3.62
6th Gear Ratio	2.64
7th Gear Ratio	1.90
8th Gear Ratio	1.38
9th Gear Ratio	1.00
10th Gear Ratio	0.74
Final Drive Ratio	3.73

APPENDIX D

See Table I.

REFERENCES

[1] B. Ran, P. J. Jin, D. Boyce, T. Z. Qiu, and Y. Cheng, "Perspectives on future transportation research: Impact of intelligent transportation system technologies on next-generation transportation modeling," *J. Intell. Transp. Syst.*, vol. 16, no. 4, pp. 226–242, 2012.

[2] K. Bengler, K. Dietmayer, B. Farber, M. Maurer, C. Stiller, and H. Winner, "Three decades of driver assistance systems: Review and future perspectives," *IEEE Intell. Transp. Syst. Mag.*, vol. 6, no. 4, pp. 6–22, Oct. 2014.

[3] K. C. Dey *et al.*, "A review of communication, driver characteristics, and controls aspects of cooperative adaptive cruise control (CACC)," *IEEE Trans. Intell. Transp. Syst.*, vol. 17, no. 2, pp. 491–509, Feb. 2016.

[4] P. Seiler, A. Pant, and K. Hedrick, "Disturbance propagation in vehicle strings," *IEEE Trans. Autom. Control*, vol. 49, no. 10, pp. 1835–1842, Oct. 2004.

[5] Y. Zhao, P. Minero, and V. Gupta, "On disturbance propagation in leader–follower systems with limited leader information," *Automatica*, vol. 50, no. 2, pp. 591–598, 2014.

[6] S. Öncü, J. Ploeg, N. van de Wouw, and H. Nijmeijer, "Cooperative adaptive cruise control: Network-aware analysis of string stability," *IEEE Trans. Intell. Transp. Syst.*, vol. 15, no. 4, pp. 1527–1537, Aug. 2014.

[7] M. di Bernardo, A. Salvi, and S. Santini, "Distributed consensus strategy for platooning of vehicles in the presence of time-varying heterogeneous communication delays," *IEEE Trans. Intell. Transp. Syst.*, vol. 16, no. 1, pp. 102–112, Feb. 2015.

[8] A. Geiger *et al.*, "Team AnnieWAY's entry to the 2011 grand cooperative driving challenge," *IEEE Trans. Intell. Transp. Syst.*, vol. 13, no. 3, pp. 1008–1017, Sep. 2012.

[9] T. Robinson, E. Chan, and E. Coelingh, "Operating platoons on public motorways: An introduction to the SARTRE platooning programme," in *Proc. 17th World Congr. Intell. Transp. Syst.*, 2010, pp. 1–12.

[10] V. Milanés, S. E. Shladover, J. Spring, C. Nowakowski, H. Kawazoe, and M. Nakamura, "Cooperative adaptive cruise control in real traffic situations," *IEEE Trans. Intell. Transp. Syst.*, vol. 15, no. 1, pp. 296–305, Feb. 2014.

[11] A. Alam, J. Mårtensson, and K. H. Johansson, "Experimental evaluation of decentralized cooperative cruise control for heavy-duty vehicle platooning," *Control Eng. Pract.*, vol. 38, pp. 11–25, May 2015.

[12] L. Zhang and G. Orosz, "Motif-based design for connected vehicle systems in presence of heterogeneous connectivity structures and time delays," *IEEE Trans. Intell. Transp. Syst.*, vol. 17, no. 6, pp. 1638–1651, Jun. 2016.

[13] J. I. Ge and G. Orosz, "Dynamics of connected vehicle systems with delayed acceleration feedback," *Transp. Res. C, Emerg. Technol.*, vol. 46, pp. 46–64, Sep. 2014.

[14] G. Orosz, "Connected cruise control: Modelling, delay effects, and nonlinear behaviour," *Vehicle Syst. Dyn.*, vol. 54, no. 8, pp. 1147–1176, 2016.

[15] Y. Zheng, S. E. Li, J. Wang, D. Cao, and K. Li, "Stability and scalability of homogeneous vehicular platoon: Study on the influence of information flow topologies," *IEEE Trans. Intell. Transp. Syst.*, vol. 17, no. 1, pp. 14–26, Jan. 2016.

[16] L. Zhang and G. Orosz, "Consensus and disturbance attenuation in multi-agent chains with nonlinear control and time delays," *Int. J. Robust Nonlinear Control*, vol. 27, no. 5, pp. 781–803, 2017.

[17] P. Setlur, J. R. Wagner, D. M. Dawson, and D. Braganza, "A trajectory tracking steer-by-wire control system for ground vehicles," *IEEE Trans. Veh. Technol.*, vol. 55, no. 1, pp. 76–85, Jan. 2006.

[18] D. Swaroop, J. K. Hedrick, and S. B. Choi, "Direct adaptive longitudinal control of vehicle platoons," *IEEE Trans. Veh. Technol.*, vol. 50, no. 1, pp. 150–161, Jan. 2001.

[19] L. Zhang, C. He, J. Sun, and G. Orosz, "Hierarchical design for connected cruise control," in *Proc. ASME Dyn. Syst. Control Conf.*, 2015, p. V001T17A005.

[20] J. Ploeg, D. P. Shukla, N. van de Wouw, and H. Nijmeijer, "Controller synthesis for string stability of vehicle platoons," *IEEE Trans. Intell. Transp. Syst.*, vol. 15, no. 2, pp. 854–865, Apr. 2014.

[21] D. Caveney, "Cooperative vehicular safety applications," *IEEE Control Syst. Mag.*, vol. 30, no. 4, pp. 38–53, Aug. 2010.

[22] L. Berezansky and E. Braverman, "On stability of some linear and nonlinear delay differential equations," *J. Math. Anal. Appl.*, vol. 314, no. 2, pp. 391–411, 2006.

[23] A. G. Ulsoy, H. Peng, and M. Çakmakci, *Automotive Control Systems*. Cambridge, U.K.: Cambridge Univ. Press, 2012.

[24] B. Bandyopadhyay, S. Janardhanan, and S. K. Spurgeon, *Advances in Sliding Mode Control: Concept, Theory and Implementation*. Berlin, Germany: Springer-Verlag, 2013.

[25] P. Ioannou and J. Sun, *Robust Adaptive Control*. Mineola, NY, USA: Courier Dover Publications, 2012.

[26] C. R. He, H. Maurer, and G. Orosz, "Fuel consumption optimization of heavy-duty vehicles with grade, wind, and traffic information," *ASME J. Comput. Nonlinear Dyn.*, vol. 11, no. 6, p. 061011, 2016.

[27] *UMTRI Safety Pilot*, accessed on Oct. 22, 2014. [Online]. Available: http://safetypilot.umtri.umich.edu/

[28] J. L. Torres, A. García, M. De Blas, and A. De Francisco, "Forecast of hourly average wind speed with ARMA models in navarre," *Solar Energy*, vol. 79, no. 1, pp. 65–77, 2005.

[29] W. B. Qin, M. M. Gomez, and G. Orosz, "Stability and frequency response under stochastic communication delays with applications to connected cruise control design," *IEEE Trans. Intell. Transp. Syst.*, vol. 18, no. 2, pp. 388–403, Feb. 2017.

[30] J.-J. E. Slotine and W. Li, *Applied Nonlinear Control*. Englewood Cliffs, NJ, USA: Prentice-Hall, 1991.

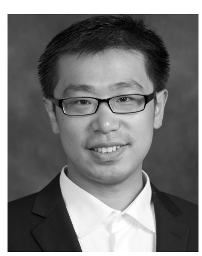

Linjun Zhang received the B.Eng. degree in automation from Northeastern University, Shenyang, China, in 2005, and the M.Eng. degree in control science and engineering from the Beijing University of Aeronautics and Astronautics, Beijing, China, in 2009. He is currently pursuing the Ph.D. degree in mechanical engineering with the University of Michigan, Ann Arbor, MI, USA.

His current research interests include intelligent transportation systems, vehicle dynamics and control, nonlinear control, time-delay systems, complex networks, and system identification.

Jing Sun (F'04) received the bachelor's and master's degrees from the University of Science and Technology of China, Hefei, China, in 1984 and 1982, respectively, and the Ph.D. degree from the University of Southern California, Los Angeles, CA, USA, in 1989.

From 1989 to 1993, she was an Assistant Professor with the Electrical and Computer Engineering Department, Wayne State University, Detroit, MI, USA. She joined the Ford Research Laboratory in 1993, where she was involved in advanced powertrain system controls. After spending almost 10 years in industry, she came back to academia in 2003 and joined the Naval Architecture and Marine Engineering Department, University of Michigan. She is currently the Michael G. Parsons Professor of Engineering with the University of Michigan, Ann Arbor, MI. She also has joint appointments in the Electrical Engineering and Computer Science Department as well as the Mechanical Engineering Department with the University of Michigan. She holds 39 U.S. patents. She has co-authored (with Petros Ioannou) a textbook on *Robust Adaptive Control*. She has authored over 200 archived journal and conference papers.

Dr. Sun was a recipient of the 2003 IEEE Control System Technology Award.

Gábor Orosz received the M.Sc. degree in engineering physics from the Budapest University of Technology, Budapest, Hungary, in 2002, and the Ph.D. degree in engineering mathematics from the University of Bristol, Bristol, U.K., in 2006.

He held post-doctoral positions with the University of Exeter, Exeter, U.K., and with the University of California at Santa Barbara, Santa Barbara, CA, USA, before joining the University of Michigan, Ann Arbor, MI, USA, in 2010, as an Assistant Professor of Mechanical Engineering. His current research interests include nonlinear dynamics and control, time-delay systems, networks, and complex systems with applications on connected and automated vehicles and biological networks.